Am J Nucl Med Mol Imaging 2016;6(2):110-119
www.ajnmmi.us /ISSN:2160-8407/ajnmmi0020537

Original Article

PET imaging of in vivo caspase-3/7 activity following myocardial ischemia-reperfusion injury with the radiolabeled isatin sulfonamide analogue [^{18}F]WC-4-116

Arun K Thukkani[1,2], Kooresh I Shoghi[1,3], Dong Zhou[1], Jinbin Xu[1], Wenhua Chu[1], Eric Novak[2], Delphine L Chen[1], Robert J Gropler[1,2], Robert H Mach[1,4,5]

[1]Mallinckrodt Institute of Radiology, Washington University School of Medicine, St. Louis, MO 63110, USA; [2]Cardiovascular Division, Washington University School of Medicine, St Louis, MO 63110, USA; Departments of [3]Biomedical Engineering, [4]Cell Biology & Physiology, [5]Biochemistry & Molecular Biophysics, Washington University School of Medicine, St. Louis, MO 63110, USA

Received November 25, 2015; Accepted February 9, 2016; Epub April 24, 2016; Published April 30, 2016

Abstract: The utility of [^{18}F]WC-4-116, a PET tracer for imaging caspase-3 activation, was evaluated in an animal model of myocardial apoptosis. [^{18}F]WC-4-116 was injected into rats at 3 hours after a 30 min period of ischemia induced by temporary occlusion of the left anterior descending coronary artery in Sprague-Dawley rats. [^{18}F]WC-4-116 uptake was quantified by 1) autoradiography, 2) microPET imaging studies, and 3) post-PET biodistribution studies. MicroPET imaging also assessed uptake of the non-caspase-3-targeted tracer [^{18}F]ICMT-18 at 3 hours post-ischemia. Enzyme assays and Western blotting assessed caspase-3 activation in both at-risk and not-at-risk regions. Caspase-3 enzyme activity increased in the at-risk but not in the not-at-risk myocardium. Quantitative autoradiographic analysis of [^{18}F]WC-4-116 demonstrated nearly 2-fold higher uptake in the ischemia-reperfusion (IR) versus sham animals. [^{18}F]WC-4-116 microPET imaging studies demonstrated that the IR animals was similarly elevated in relation to sham. [^{18}F]ICMT-18 uptake did not increase in at-risk myocardium despite evidence of caspase-3 activation. Biodistribution studies with [^{18}F]WC-4-116 confirmed the microPET findings. These data indicate that the caspase-3-PET tracer [^{18}F]WC-4-116 can noninvasively image *in vivo* caspase activity during myocardial apoptosis and may be useful for clinical imaging in humans.

Keywords: Isatin sulfonamide analogue, apoptosis, PET, tracer, caspase

Introduction

Apoptosis is a highly regulated, adenosine triphosphate (ATP)-dependent cellular death program that plays a crucial role during embryonic development, maintenance of the immune system, and tissue homeostasis [1]. Two independent pathways can mediate this process. Stimuli such as ischemia-reperfusion (IR) injury activate the intrinsic apoptotic pathway that involves mitochondrial permeabilization leading to cytochrome c release and caspase-9 activation. In contrast, cytokines and other factors such as the Fas ligand or tumor necrosis factor-alpha bind to external cell receptors to activate the extrinsic pathway, leading to caspase-8 activation. Both caspase-8 and caspase-9 lead to activation of the executioner caspases, caspase-3 and -7. These latter caspases are responsible for mediating the hallmark physiologic and morphologic cellular changes of cells undergoing apoptosis; specifically, cytoplasmic and nuclear condensation, DNA fragmentation, membrane blebbing, as well as phosphatidylserine (PS) externalization on the outer leaflet of the plasma membrane [2, 3]. These pathways as they relate to imaging have been recently reviewed [4].

Over the past decade, dysregulated apoptosis has been implicated in a wide spectrum of clinically important diseases [5, 6]. The importance of apoptotic cell death in cardiovascular disease is also increasingly being recognized.

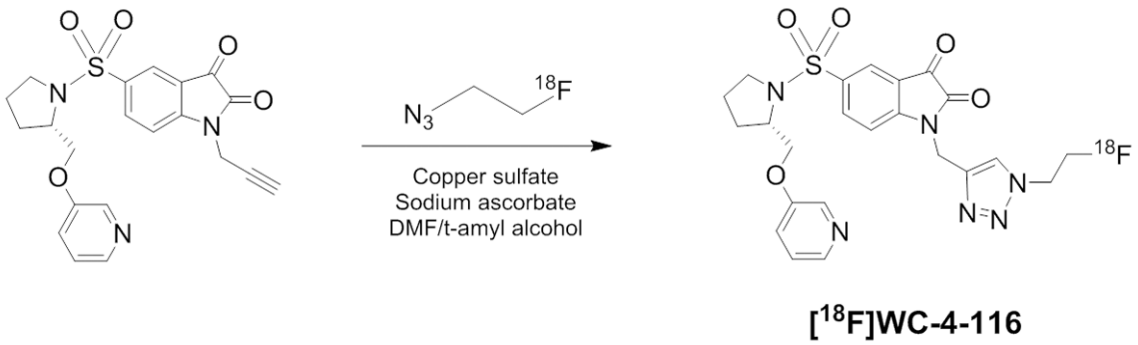

Figure 1. Radiosynthesis scheme for [^{18}F]WC-4-116.

Increased cardiomyocyte apoptosis has been noted in ischemic and non-ischemic cardiomyopathies, atherosclerosis, and cardiac allograft rejection [7-10]. Following prolonged myocardial ischemia, cardiomyocyte necrosis predominates. However, with timely reperfusion, increased levels of apoptosis have been detected [11, 12], at which time caspase inhibition may preserve myocytes, reducing infarct size and potentially protecting cardiac function [13, 14]. Thus, noninvasive means of detecting apoptosis *in vivo* may be useful tools for assessing the degree of apoptosis both to assess for potential intervention efficacy and to study the factors that contribute to increased apoptosis vs necrosis [15, 16].

A number of approaches have been developed to image apoptosis in vivo [4]. However, most of these methods do not measure apoptosis specifically. SPECT- and PET-based tracers have targeted annexin V, a 37 kDA protein that binds to externalized phosphatidylserine (PS) residues expressed only on apoptotic cells [17-19], but these tracers can also detect PS residues in necrotic cells as a results of cell membrane breakdown [20]. The targeting specificity of both radiolabeled amphipathic small molecule PET tracers, like [^{18}F]ML-10 [21], and the MRI agent superparamagnetic iron oxide (SPIO)-labeled synaptogamin, for apoptotic cells [22] has also been questioned. Therefore, radiolabeled small-molecule PET imaging agents that bind to more apoptosis-specific targets will potentially improve upon these existing imaging approaches.

Isatin sulfonamide analogs are potent inhibitors of caspase-3 and -7 [23] that have been radiolabeled for PET imaging [24]. Initial microPET imaging studies have shown that these analogs readily detect both hepatic and chemotherapy-induced tumor apoptosis [25-27]. [^{18}F]WC-4-116 is a second generation radiolabeled isatin sulfonamide analogue with enhanced potency for the executioner caspases (~4.5 nM and ~3.8 nM for caspase-3 and -7 respectively [24]. Given the importance of apoptosis in cardiac disease, we sought to assess the ability of [^{18}F]WC-4-116 to image caspase-3/7 activity as a marker of ischemia-induced apoptosis using a modified version of a well-characterized rat cardiac ischemia-reperfusion model induced by left anterior descending (LAD) ligation [28].

Materials and methods

Synthesis of [^{18}F]WC-4-116 and [^{18}F]ICMT-18

The tracers [^{18}F]WC-4-116 and [^{18}F]ICMT-18 were synthesized from the corresponding alkyne precursors as previously published [25, 29, 30]. The radiosynthetic scheme for [^{18}F]WC-4-116 is shown in **Figure 1**. Briefly, a solution of alkyne precursor in DMF was added to a solution 2-[^{18}F] fluoroethyl azide, synthesized and distilled in *t*-amyl alcohol, followed by the addition of a mixture of $CuSO_4 \cdot 5H_2O$ and sodium ascorbate in water. The reaction mixture was allowed to react at room temperature for 10 min, and standard solid phase extraction methods were used to remove *t*-amyl alcohol and other salts. The tracer was purified by reversed phase HPLC. All radiolabeling was done manually. The isolated yields from the radiosynthesis were typically 20-30% (not decay-corrected), with radiochemical purity >99%, and specific activity of 1-2 Ci/μMol. In vitro caspase inhibition by [^{18}F]ICMT-18 was confirmed using previously described methods that are detailed in the

supplement [31]. Cell uptake studies conducted as previously described [24] and detailed in the supplement also confirmed [^{18}F]WC-4-116 specificity for binding caspase-3.

Animal groups, in vivo LAD coronary artery ligation, and myocardial tissue harvest

All animal procedures were conducted in accordance with guidelines published in the *Guide for the Care and Use of Laboratory Animals* and were approved by the Animal Studies Committee of the Washington University School of Medicine. Temporary ligation of the LAD or sham surgery was performed on male Sprague-Dawley rats (9-11 weeks of age, 275-300 g, Charles River Laboratories) as previously described [32]. During the procedure, the suture passed under the LAD was tied for 30 min to induce ischemia followed by release to allow reperfusion (ischemia-reperfusion, IR, group) or left in place without tying for the sham surgeries (SS group). Immediately after the suture was released to restore perfusion, the chest was closed. Following the surgical procedure, the animals were weaned from ventilator support with reversal agent (atipamezole, 1 mg/kg SC) administered to hasten recovery.

For myocardial tissue harvest, animals were reanesthetized with 1-2% isoflurane at 3 hours after ligation, and the thorax was reopened to tie off the LAD, producing distal blanching. Evan's Blue dye (5% in saline; Sigma-Aldrich) was injected via tail vein to delineate the myocardial at-risk region. The hearts were quickly excised, the unstained at-risk and stained not at-risk myocardium were separated, snap-frozen in liquid nitrogen, and stored at -80°C for *in vitro* analysis. Caspase-3 activation was confirmed at 3 hours after reperfusion (i.e. 3 hours after release of the tied suture, N = 5 IR group, N = 3 SS group) using the methods described below (Supplemental Figure 1). This time point was thus used for all tracer studies. Myocardial tissue was also obtained from the animals used for autoradiography (N = 3 per group) and microPET imaging experiments (N = 4 per group except for N = 3 in the IR group imaged with [^{18}F]ICMT-18).

Fluorometric assay and western immunoblotting for caspase-3/7 activity and expression.

Caspase-3/7 activity was assayed in the at-risk and not at-risk myocardial samples as previously published [27]. In brief, 200 mg of protein from homogenized myocardial tissue in the presence or absence of caspase-3/7 inhibitor (1 mM Ac-DEVD-CHO; Sigma-Aldrich) was incubated in assay buffer containing caspase-3/7 substrate (20 mM AC-DVED-AMC; Biomol International). Fluorescence was measured every hour for 8 hr, plotted, and linear regression applied to determine the rate of caspase-3 activity in units of amido-4-methylcoumarin (AMC) produced per min per mg protein.

For caspase-3 western immunoblotting, 100 μg of protein was subjected to SDS-PAGE using 4-15% Tris-HCl for ~90 min at 100 V followed by the protein transfer to Immobilon P membrane (Millipore, Inc). After blocking with 5% milk in Tris-buffered saline for 1 hr, the membrane was probed with anti-caspase-3 primary antibody (1:1000; Cell Signaling) overnight at 4°C, washed, blotted with peroxidase-conjugated secondary antibody (1:10,000), washed, then developed (SuperSignal West Dura, Thermo Scientific).

*Ex vivo autoradiography with [^{18}F]*WC-4-116 *and [^{18}F]*ICMT-18

After the 3 hr reperfusion interval, IR and SS animals (N = 3 per group) were injected with ~1-1.5 mCi of [^{18}F]WC-4-116 or [^{18}F]ICMT-18 via tail vein under isoflurane anesthesia. Myocardial tissue, harvested as described above, was sliced in 1 mm axial sections and measured over 80 minutes for autoradiographic determination of tracer distribution (Packard InstantImager). Corresponding photographic images of these stained sections were then obtained using a flatbed scanner (Hewlett Packard). The accumulated regional radioactivity of the at-risk and not at-risk regions, expressed as a ratio of the counts in the at-risk vs not-at-risk regions (counts/mm$^2_{\text{at-risk}}$: counts/mm$^2_{\text{f}}$) was determined for animals in each treatment group.

MicroPET imaging protocol

The animals were anesthetized with 1-2% isoflurane and imaged with an Inveon microPET/CT scanner (Siemens, Knoxville, TN). After obtaining CT images for attenuation correction, the dynamic PET acquisition started at five seconds after tracer injection. A 10-minute dynamic microPET image acquisition with [^{15}O]H_2O

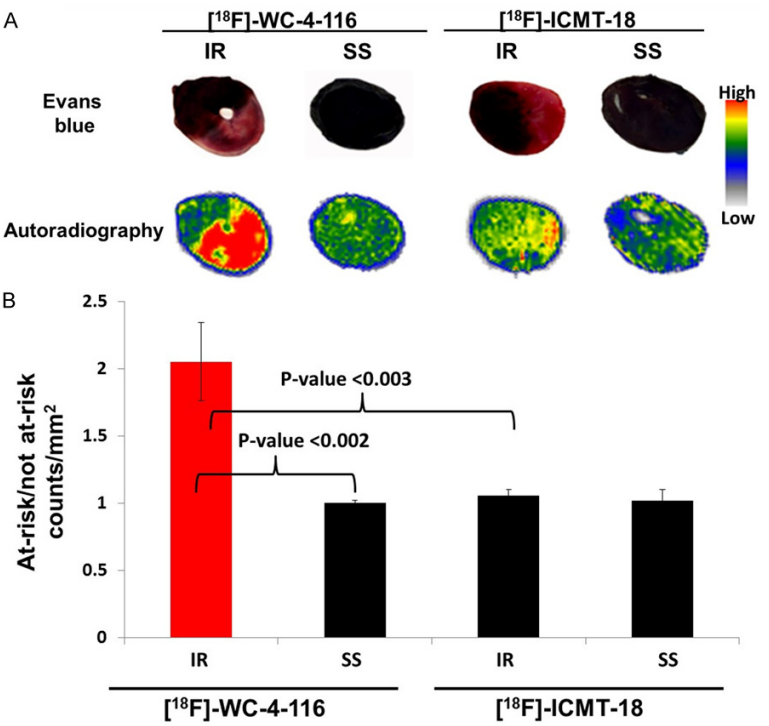

Figure 2. Autoradiography of IR and SS animals administered the tracers [^{18}F]WC-4-116 or [^{18}F]ICMT-18 and representative Evan's Blue stained cardiac sections (A) Quantitation of tracer accumulation from autoradiography studies (counts/mm^2) of the at-risk and not at-risk myocardial regions are shown graphically (B). Bonferroni-adjusted *p*-values for pair-wise comparisons are indicated.

(500-700 μCi) to quantify myocardial blood flow (MBF) was performed followed by a 30 min dynamic acquisition with either [^{18}F]WC-4-116 or [^{18}F]ICMT-18 (400-500 μCi). Following microPET imaging, the at-risk and not at-risk regions were excised as described above for gamma counting and caspase-3 activity assessment. Images were reconstructed using a fast maximum a posteriori (fastMAP) algorithm implemented by Siemens Inc with a CT-based attenuation correction. The following frame binning schedule was used in the reconstruction: 24 × 5 sec, 8 × 60 sec, 6 × 180 sec, and 4 × 300 sec.

Image analysis and quantification

The left-ventricle blood pool (LVBP) was localized by summing early frames (typically the first 10 frames) of [^{18}F]WC-4-116 or [^{18}F]ICMT-18 images (see Supplemental Figure 2 for blood pool images). A region of interest (ROI) was drawn on LVBP and overlaid onto [^{15}O]H_2O images to reconstruct the arterial input function [33]. Similarly, the at-risk region of the LV myocardium was identified adjacent to LVBP from the sum of the last 10 min of imaging with [^{18}F]WC-4-116 (Supplemental Figure 2). Because the left ventricular wall could not be visualized with [^{18}F]ICMT-18, the LVBP images were used as a reference to place ROIs in a similar location as with the [^{18}F]WC-4-116 images to correspond to the ventricular wall. A region in the superior half of the LV wall representing the not at-risk myocardium was identified in a similar manner. ROIs circumscribing these respective areas were utilized to generate time-activity curves for at-risk and not at-risk regions respectively. We observed significant spill-over from both the right and left ventricles (RV and LV, respectively) into the reference region, in particular at early time points. At late time points, however, there is uniform activity in the reference region, LV, and RV with high signal only in the at-risk region. For this reason, we chose to display the data as the ratio of standard uptake value (SUV) of at-risk to not-at-risk regions. The myocardial blood flow (MBF) in the at-risk region of each imaged animal was quantified by optimizing a mathematical model for [^{15}O]H_2O [34].

Biodistribution studies

Tracer biodistribution in the myocardium was further confirmed for all animals undergoing microPET imaging. After completing the microPET imaging session, the at-risk and not at-risk myocardium were harvested, weighed, and immediately frozen on dry ice. These sections were counted separately by Beckman Gamma 8000 well counter while frozen and then later assayed for caspase-3 enzyme activity (as above). The percent-injected dose per gram of tissue (%ID/g) was determined for each sample and $\%ID/g_{at\text{-}risk}$: $\%ID/g_{not\ at\text{-}risk}$ was determined for each treatment.

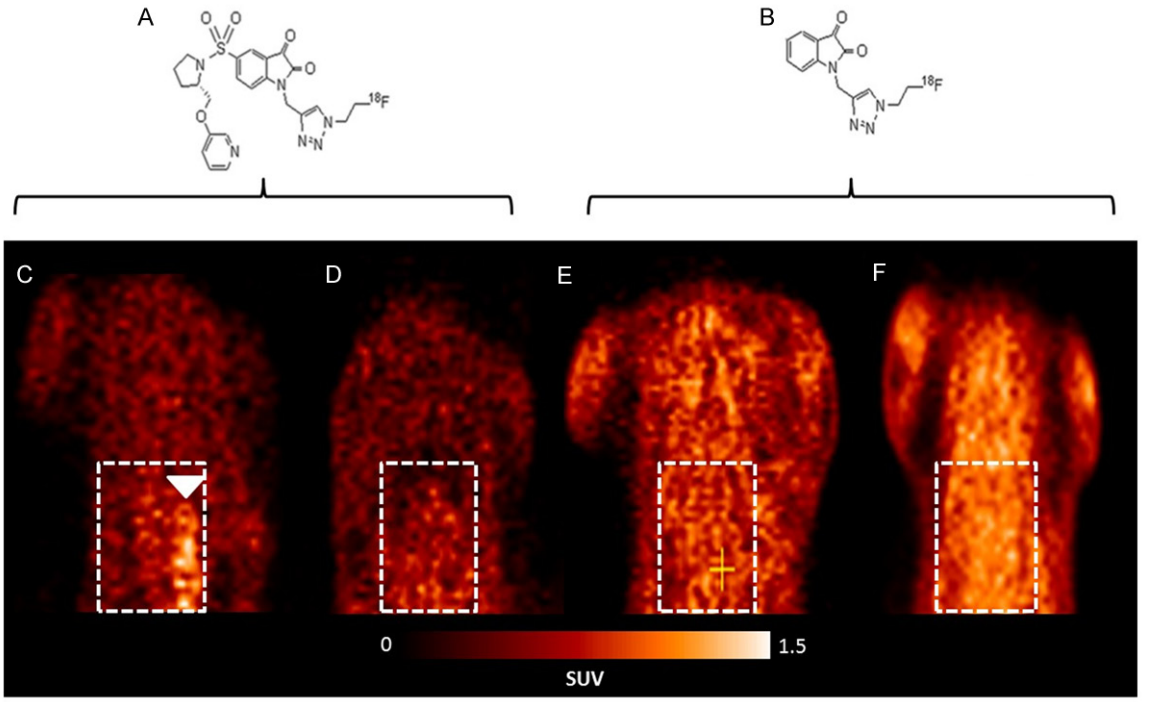

Figure 3. MicroPET imaging of IR and SS animals with the tracers [^{18}F]WC-4-116 and [^{18}F]ICMT-18. (A) Structure of [^{18}F]WC-4-116. (B) Structure of [^{18}F]ICMT-18. (C-F) Representative late summed microPET images of IR and SS animals imaged with [^{18}F]WC-4-116 (C, D) or [^{18}F]ICMT-18 (E, F). [^{18}F]WC-4-116 microPET imaging demonstrates LV tracer uptake in IR (panel C) but not SS animals (D). Images of IR (E) and SS (F) animals administered [^{18}F]ICMT-18 demonstrate no focal myocardial accumulation of this tracer. White boxes denote cardiac position; white arrowhead indicates LV uptake.

Statistical methods

Differences in at-risk myocardial caspase-3/7 activity for model validation studies between IR and SS treatments were analyzed using the two-sided Student's t-test as were differences in mean SUV or %ID/g between groups. For all other data, a two-way ANOVA analysis with interaction was conducted to identify the effects of tracer and treatment on at-risk myocardial caspase-3/7 activity, at-risk myocardial blood flow, $SUV_{at\text{-}risk}$: $SUV_{not\ at\text{-}risk}$, %ID/$g_{at\text{-}risk}$: %ID/$g_{not\ at\text{-}risk}$ from animals undergoing microPET imaging and counts/$mm^2{}_{at\text{-}risk}$: counts/$mm^2{}_{not\ at\text{-}risk}$ derived from the autoradiography studies. Significance was identified at the alpha level of 5% ($\alpha = 0.05$) for all statistical analyses. A significant interaction indicates that the effect of treatment on the index varies with respect to tracer (or vice-versa). Following a significant interaction, post-hoc analyses were conducted testing all pair-wise comparisons of tracer and treatment combinations. Bonferroni-adjusted post-hoc results were reported. All analysis was conducted in SAS® v9.3 (SAS Institute, Inc., Cary, NC).

Results

In vitro studies and model validation

The inability of [^{18}F]ICMT-18 to inhibit caspase-3 activation was confirmed in vitro (Supplemental Figure 3). Staurosporine treated HeLa cells demonstrated increased [^{18}F]WC-4-116 uptake that was blocked up to 50% or greater with cold WC-4-116 (Supplemental Figure 4).

Autoradiography studies

Autoradiography demonstrated substantial [^{18}F]WC-4-116 accumulation localized to the at-risk myocardium as demarcated by dye staining (**Figure 2A**). In contrast, no significant accumulation of [^{18}F]WC-4-116 was seen with SS treatment (**Figure 2B**). Cardiac sections from animals administered [^{18}F]ICMT-18 demonstrated no significant accumulation in the unstained

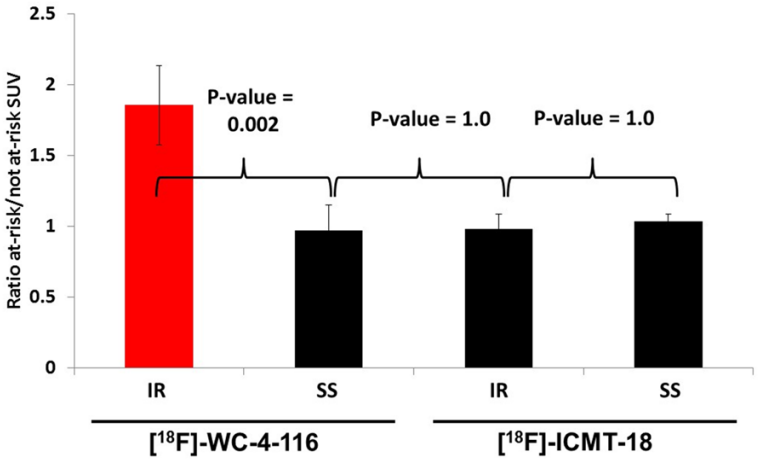

Figure 4. SUV analysis of microPET images. Mean SUV of the at-risk and not at-risk myocardial regions of the experimental imaging groups were measured and the mean ratio of $SUV_{at\text{-}risk}$: $SUV_{not\ at\text{-}risk}$ (± standard error) was derived. All treatments are n = 4 except for the IR group imaged with [^{18}F]ICMT-18 (n = 3) with a *p*-value (ANOVA) = 0.002 for interaction between tracer and treatment type. Bonferroni-adjusted *p*-values for pair-wise comparisons are indicated.

ventricular at-risk region in the IR, which appeared similar to that seen in the SS animals without any at-risk myocardium.

[^{18}F]WC-4-116 accumulation, based on autoradiographic quantitation of regional tracer accumulation expressed as counts/$mm^2_{at\text{-}risk}$: counts/$mm^2_{not\ at\text{-}risk}$ was significantly higher in IR than SS animals (2.05 ± 0.17 versus 1.00 ± 0.01; p < .001), shown in **Figure 2B**. No difference was found in [^{18}F]ICMT-18 uptake between the IR and SS animals (1.06 ± 0.02 and 1.02 ± 0.05 respectively, p = 1.00). The difference in counts/$mm^2_{at\text{-}risk}$: counts/$mm^2_{not\ at\text{-}risk}$ between IR and SS was also greater for [^{18}F]WC-4-116 than for [^{18}F]ICMT-18 (p < 0.001).

In vivo detection of myocardial apoptosis with [^{18}F]WC-4-116 microPET imaging studies

Representative late summed images from 30 min dynamic microPET imaging studies of IR and SS animals administered [^{18}F]WC-4-116 or [^{18}F]ICMT-18 are shown in **Figure 3**. As observed with autoradiography, microPET images of IR animals imaged with [^{18}F]WC-4-116 demonstrated tracer accumulation in the LV free wall corresponding to the at-risk IR myocardial zone that was not observed in the SS group (**Figure 3**). While more nonspecific binding was seen diffusely when [^{18}F]ICMT-18 imaging was performed, neither IR nor SS animals showed tracer accumulation in the at-risk LV myocardium when compared with IR animals imaged with [^{18}F]WC-4-116.

SUV analysis of the late summed images from the dynamic microPET scans of the four groups confirmed the visual assessment of the images. The average SUV of the at-risk LV region for [^{18}F]WC-4-116 was higher than the not-at-risk myocardium in IR animals (0.81 versus 0.46, respectively; p = 0.012) but not in SS animals (0.49 at-risk versus 0.51 not-at-risk; p = 0.92). $SUV_{at\text{-}risk}$: $SUV_{not\ at\text{-}risk}$ (i.e. SUV_{target}: $SUV_{reference}$) for the IR animals was significantly higher than in SS animals. The average SUVs for [^{18}F]ICMT-18 in at-risk and not-at-risk myocardium did not differ between IR and SS animals, yielding $SUV_{at\text{-}risk}$: $SUV_{not\ at\text{-}risk}$ ratios that near unity (**Figure 4**). $SUV_{at\text{-}risk}$: $SUV_{not\ at\text{-}risk}$ ratios for [^{18}F]WC-4-116 were significantly higher than those for [^{18}F]ICMT-18 in at-risk myocardial tissue (p = 0.002 for interaction). Representative time-activity curves from the microPET imaging studies are shown in Supplemental Figure 5.

Post-microPET biodistribution studies

In the [^{18}F]WC-4-116 imaging groups, the %ID/g of the at-risk myocardial samples from the IR animals was more than twice that of the SS animals (0.14 ± 0.01 versus 0.05 ± 0.01; p < 0.05). In contrast, the accumulated radioactivity content of the not at-risk myocardium from these two treatments was not statistically different (0.07 ± 0.01 versus 0.05 ± 0.01; p = 0.28). Accordingly, $\%ID/g_{at\text{-}risk}$: $\%ID/g_{not\ at\text{-}risk}$ was significantly higher in IR vs SS animals (p = 0.003; **Figure 5**). The %ID/g of the at-risk and not-at-risk myocardium for SS and IR animals undergoing [^{18}F]ICMT-18 microPET were both higher relative to that measured with [^{18}F]WC-4-116; however, $\%ID/g_{at\text{-}risk}$: $\%ID/g_{not\ at\text{-}risk}$ for these experimental groups did not differ (p = 1.00). The difference in $\%ID/g_{at\text{-}risk}$: $\%ID/g_{not\ at\text{-}risk}$ between IR and SS was significantly greater for [^{18}F]WC-4-116 and [^{18}F]ICMT-18 (p = 0.003).

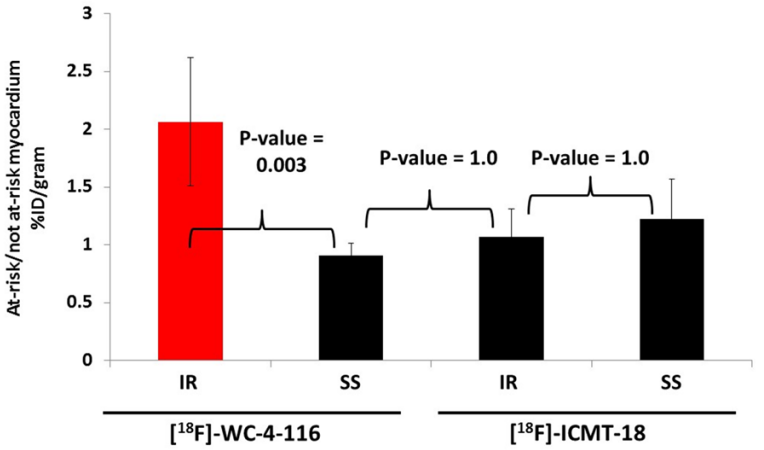

Figure 5. Biodistribution studies. %ID/g of the at-risk and not at-risk myocardial samples derived from the experimental imaging groups was measured and the mean ratio of $\%ID/g_{at\text{-}risk}$: $\%ID/g_{not\ at\text{-}risk}$ (± standard error) was derived. All treatments are n = 4 except for the SS group imaged with [^{18}F]ICMT-18 (n = 3) with a *p*-value (ANOVA) = 0.003 for interaction between tracer and treatment type. Bonferroni-adjusted *p*-values for pair-wise comparisons are indicated.

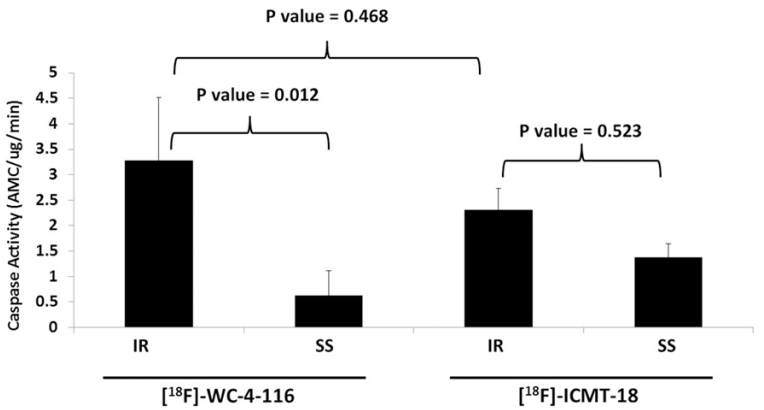

Figure 6. *Ex vivo* analysis of at-risk myocardial caspase-3/7 activity of IR and SS animals undergoing tracer microPET imaging. Mean caspase-3/7 activity (± standard error) of the at-risk ventricular samples isolated from the experimental imaging groups was measured by *ex vivo* fluorometric assay. All treatments are n = 4 with a *p*-value (ANOVA) = 0.033 for interaction between tracer and treatment type. Bonferroni-adjusted *p*-values for pair-wise comparisons are indicated.

Ex vivo analysis of myocardial caspase-3/7

The caspase-3 activity of the at-risk LV myocardium in all IR animals imaged by microPET increased compared to SS animals (**Figure 6**), confirming the results from the validation studies (shown in Supplemental Figure 1).

Discussion

Isatin sulfonamide analogues are potent, membrane-permeable inhibitors of caspases [23]. We and others have developed radiolabeled isatin sulfonamide analogues with enhanced specificity for the executioner caspases and greater membrane permeability [24, 25, 35]. Thus, these tracers have the advantage of targeting enzymes that are specifically activated by the apoptotic cascade, unlike other approaches which may image apoptosis but will also likely image cells dying by necrosis as well [17-19]. These functionalized small molecules have been utilized as tracers for microPET imaging studies detecting *in vivo* apoptosis in chemotherapy-, cycloheximide-, and Fas antibody-induced murine models of apoptosis [25-27]. The present study expands upon this by describing the first application of one of these analogues, [^{18}F]WC-4-116, to detect *in vivo* apoptosis noninvasively in a clinically relevant model of ischemia-reperfusion cardiovascular disease.

Our quantitative analysis of autoradiography, microPET imaging, and biodistribution study results with [^{18}F]WC-4-116 consistently demonstrated that [^{18}F]WC-4-116 accumulates only in at-risk myocardium regions that have increased levels of apoptosis. By all three approaches, we demonstrated an approximately 2-fold increase in [^{18}F]WC-4-116 accumulation when comparing at-risk to not-at-risk myocardium. We used immunoblotting studies as well as measurements of caspase-3 activity using a standard fluorometric enzyme assay to assess the degree of caspase-3 activation in at-risk myocardium where [^{18}F]WC-4-116 accumulates in this model. These assays confirmed that caspase-3 activation occurred only in areas where [^{18}F]WC-4-116 accumulated. Thus, these data support our hypothesis that [^{18}F]

WC-4-116 can be used to image caspase-3 activation in this model.

We further confirmed the specificity of [^{18}F]WC-4-116 for caspase-3 activity by using a non-caspase-3 targeted tracer, [^{18}F]ICMT-18, to demonstrate that this similarly structured tracer did not accumulate in regions of increased caspase-3 activity. [^{18}F]ICMT-18 has been used in cancer-chemotherapy models as a negative control for imaging caspase-3 activation [25]. Therefore, we chose to use this approach as well because the delivery of a non-targeted, structurally similar tracer should depend only on blood flow and would best reflect the delivery of [^{18}F]WC-4-116 but without the effect of targeted binding. IR animals imaged with [^{18}F]ICMT-18 had elevated myocardial caspase-3/7 activity as expected from the model, but none of the quantitative analyses for [^{18}F]ICMT-18 uptake in *ex vivo* autoradiography, microPET images, and tissues assessed in the biodistribution studies, demonstrated significant [^{18}F]ICMT-18 accumulation in at-risk myocardial regions. Collectively, these lines of evidence support the utility of [^{18}F]WC-4-116 to image *in vivo* caspase-3/7 activity specifically in apoptotic myocardium. These results support further study of [^{18}F]WC-116 to images apoptosis *in vivo*.

Prior studies have demonstrated that compared with normal myocardium, the blood flow of IR myocardium is diminished [36]. Indeed, [^{15}O]H_2O microPET imaging confirmed the development of significantly reduced regional blood flow of the at-risk LV myocardium in the IR but not SS animals (see Supplemental Figure 6). Thus, our use of [^{18}F]ICMT-18 further enabled us to confirm that [^{18}F]WC-4-116 accumulation in the IR animals was due to *in vivo* targeting of activated caspases rather than nonspecific retention as a result of delayed washout from regionally diminished blood flow. Our data demonstrate that at-risk myocardium with confirmed increased caspase-3 activation and diminished blood flow did not retain [^{18}F]ICMT-18 more than not-at-risk myocardium, in contrast to [^{18}F]WC-4-116, which was retained under similar conditions. Therefore, these data further strengthen our hypothesis that [^{18}F]WC-4-116 can be used to detect apoptotic cell death in the setting of ischemia-reperfusion injury.

One of the primary limitations of this approach is the potential lack of sensitivity for detecting caspase-3 activation in patients with ischemia reperfusion myocardial injury. While our tracer may be useful for determining the amount of myocardium that could be salvaged after interventions such as cardiac stenting or bypass grafting, we do not have data to know whether the tracer can measure clinically significant differences in patients. In considering clinical applications, the degree of apoptosis in at-risk myocardium in *patients* is in fact not known because no tools have been available to make such measurements easily in patients. Therefore, the development of tools such as [^{18}F]WC-4-116 will actually enable investigators to begin making such measurements and determine whether clinically relevant levels of apoptosis can be detected in patients with tracers like [^{18}F]WC-4-116 in patients. Additionally, even if the clinical application of [^{18}F]WC-4-116 is limited, the use of [^{18}F]WC-4-116 in patients could still help drive clinical research applications in which dynamic imaging could be performed for more sophisticated quantitative analyses. Conducting clinical trials with this tracer will thus best assess the full potential of this tracer.

Conclusion

The current studies utilizing the LAD ligation model of myocardial IR injury demonstrate that the radiolabeled isatin sulfonamide analogue [^{18}F]WC-4-116, a functionalized small molecule PET tracer specifically targeting the activated caspases-3 and -7, is capable of detecting increased activity levels of these executioner caspases in apoptotic myocardium *in vivo*. Therefore, [^{18}F]WC-4-116 represents a promising candidate tracer for further translational study to detect apoptosis for clinical imaging applications.

Acknowledgements

The authors thank the Washington University School of Medicine Cyclotron Facility for ^{18}F production and the Small Animal Imaging Core for conducting the microPET studies. The authors would also like to thank Justin Rothfuss for his excellent technical assistance.

Disclosure of conflict of interest

None.

Address correspondence to: Dr. Robert H Mach, Department of Radiology, Perelman School of Medicine, University of Pennsylvania, Philadelphia, PA 19104, USA. Tel: 215-746-8233; Fax: 215-746-0002; E-mail: rmach@mail.med.upenn.edu

References

[1] Taylor RC, Cullen SP and Martin SJ. Apoptosis: Controlled demolition at the cellular level. Nat Rev Mol Cell Biol 2008; 9: 231-241.

[2] Slee EA, Adrain C and Martin SJ. Executioner caspase-3, -6, and -7 perform distinct, non-redundant roles during the demolition phase of apoptosis. J Biol Chem 2001; 276: 7320-7326.

[3] Balasubramanian K, Mirnikjoo B and Schroit AJ. Regulated externalization of phosphatidylserine at the cell surface. J Biol Chem 2007; 282: 18357-18364.

[4] Niu G and Chen X. Apoptosis imaging: beyond annexin V. J Nucl Med 2010; 51: 1659-1662.

[5] Yang Q, Underwood MJ, Hsin MKY, Liu XC and He GW. Dysfunction of pulmonary vascular endothelium in chronic obstructive pulmonary disease: Basic considerations for future drug development. Curr Drug Metab 2008; 9: 661-667.

[6] Friedlander RM. Apoptosis and caspases in neurodegenerative diseases. N Engl J Med 2003; 348: 1365-1375.

[7] Narula J, Haider N, Virmani R, DiSalvo TG, Kolodgie FD, Hajjar RJ, Schmidt U, Semigran MJ, Dec GW and Khaw B-A. Apoptosis in myocytes in end-stage heart failure. N Engl J Med 1996; 335: 1182-1189.

[8] Olivetti G, Abbi R, Quaini F, Kajstura J, Cheng W, Nitahara JA, Quaini E, Di Loreto C, Beltrami CA, Krajewski S, Reed JC and Anversa P. Apoptosis in the failing human heart. N Engl J Med 1997; 336: 1131-1141.

[9] Isner JM, Kearney M, Bortman S and Passeri J. Apoptosis in human atherosclerosis and restenosis. Circulation 1995; 91: 2703-2711.

[10] Gopal S, Narasimhan U, Day JD, Gao R, Kasper EK, Chen C-L, Cina S, Robertson AL and Hruban RH. The Quilty lesion enigma: Focal apoptosis/necrosis and lymphocyte subsets in human cardiac allografts. Pathol Int 1998; 48: 191-198.

[11] Monassier JP. Reperfusion injury in acute myocardial infarction. From bench to cath lab. Part I: Basic considerations. Arch Cardiovasc Dis 2008; 101: 491-500.

[12] Monceau V, Belikova Y, Kratassiouk G, Robidel E, Russo-Marie F and Charlemagne D. Myocyte apoptosis during acute myocardial infarction in rats is related to early sarcolemmal translocation of annexin A5 in border zone. Am J Physiol Heart Circ Physiol 2006; 291: H965-H971.

[13] Holly TA, Drincic A, Byun Y, Nakamura S, Harris K, Klocke FJ and Cryns VL. Caspase inhibition reduces myocyte cell death induced by myocardial ischemia and reperfusion in vivo. J Mol Cell Cardiol 1999; 31: 1709-1715.

[14] Kovacs P, Bak I, Szendrei L, Vecsernyes M, Varga E, Blasig IE and Tosaki A. Non-specific caspase inhibition reduces infarct size and improves post-ischaemic recovery in isolated ischaemic/reperfused rat hearts. Naunyn Schmiedebergs Arch Pharmacol 2001; 364: 501-507.

[15] Chang J, Ormerod M, Powles TJ, Allred DC, Ashley SE and Dowsett M. Apoptosis and proliferation as predictors of chemotherapy response in patients with breast carcinoma. Cancer 2000; 89: 2145-2152.

[16] Haimovitz-Friedman A, Yang TJ, Thin TH and Verheij M. Imaging radiotherapy-induced apoptosis. Radiat Res 2012; 177: 467-482.

[17] Zijlstra S, Gunawan J and Burchert W. Synthesis and evaluation of a ^{18}F-labelled recombinant annexin-V derivative, for identification and quantification of apoptotic cells with PET. Appl Radiat Isot 2003; 58: 201-207.

[18] Blankenberg FG, Katsikis PD, Tait JF, Davis RE, Naumovski L, Ohtsuki K, Kopiwoda S, Abrams MJ, Darkes M, Robbins RC, Maecker HT and Strauss HW. In vivo detection and imaging of phosphatidylserine expression during programmed cell death. Proc Natl Acad Sci U S A 1998; 95: 6349-6354.

[19] Boersma HH, Kietselaer BLJH, Stolk LML, Bennaghmouch A, Hofstra L, Narula J, Heidendal GAK and Reutelingsperger CPM. Past, present, and future of Annexin A5: From protein discovery to clinical applications. J Nucl Med 2005; 46: 2035-2050.

[20] Niu G and Chen X. Apoptosis imaging: Beyond Annexin V. J Nucl Med 2010; 51: 1659-1662.

[21] Grimberg H, Levin G, Shirvan A, Cohen A, Yogev-Falach M, Reshef A and Ziv I. Monitoring of tumor response to chemotherapy in vivo by a novel small-molecule detector of apoptosis. Apoptosis 2009; 14: 257-267.

[22] Zhao M, Beauregard DA, Loizou L, Davletov B and Brindle KM. Non-invasive detection of apoptosis using magnetic resonance imaging and a targeted contrast agent. Nat Med 2001; 7: 1241-1244.

[23] Lee D, Long SA, Adams JL, Chan G, Vaidya KS, Francis TA, Kikly K, Winkler JD, Sung CM, Debouck C, Richardson S, Levy MA, DeWolf WE, Keller PM, Tomaszek T, Head MS, Ryan MD, Haltiwanger RC, Liang PH, Janson CA, McDevitt PJ, Johanson K, Concha NO, Chan W, Abdel-Meguid SS, Badger AM, Lark MW, Nadeau DP, Suva LJ, Gowen M and Nuttall ME. Potent and selective nonpeptide inhibitors of caspases 3 and 7 inhibit apoptosis and maintain cell func-

tionality. J Biol Chem 2000; 275: 16007-16014.
[24] Chu W, Rothfuss J, Zhou D and Mach RH. Synthesis and evaluation of isatin analogs as caspase-3 inhibitors: Introduction of a hydrophilic group increases potency in a whole cell assay. Bioorg Med Chem Lett 2011; 21: 2192-2197.
[25] Nguyen QD, Smith G, Glaser M, Perumal M, Årstad E and Aboagye EO. Positron emission tomography imaging of drug-induced tumor apoptosis with a caspase-3/7 specific [^{18}F]-labeled isatin sulfonamide. Proc Natl Acad Sci U S A 2009; 106: 16375-16380.
[26] Chen DL, Zhou D, Chu W, Herrbrich P, Engle JT, Griffin E, Jones LA, Rothfuss JM, Geraci M, Hotchkiss RS and Mach RH. Radiolabeled isatin binding to caspase-3 activation induced by anti-Fas antibody. Nucl Med Biol 2012; 39: 137-144.
[27] Chen DL, Zhou D, Chu W, Herrbrich PE, Jones LA, Rothfuss JM, Engle JT, Geraci M, Welch MJ and Mach RH. Comparison of radiolabeled isatin analogs for imaging apoptosis with positron emission tomography. Nucl Med Biol 2009; 36: 651-658.
[28] Yaoita H, Ogawa K, Maehara K and Maruyama Y. Attenuation of ischemia/reperfusion injury in rats by a caspase inhibitor. Circulation 1998; 97: 276-281.
[29] Zhou D, Chu W, Dence CS, Mach RH and Welch MJ. Highly efficient click labeling using 2-[^{18}F] fluoroethyl azide and synthesis of an ^{18}F *N*-hydroxysuccinimide ester as conjugation agent. Nucl Med Biol 2012; 39: 1175-1181.
[30] Chen DL, Engle JT, Griffin EA, Miller JP, Chu W, Zhou D and Mach RH. Imaging caspase-3 activation as a marker of apoptosis-targeted treatment response in cancer. Mol Imaging Biol 2015; 17: 384-393.
[31] Chu W, Rothfuss J, d'Avignon A, Zeng C, Zhou D, Hotchkiss RS and Mach RH. Isatin sulfonamide analogs containing a Michael addition acceptor: a new class of caspase 3/7 inhibitors. J Med Chem 2007; 50: 3751-3755.
[32] Thukkani AK, Martinson BD, Albert CJ, Vogler GA and Ford DA. Neutrophil-mediated accumulation of 2-ClHDA during myocardial infarction: 2-ClHDA-mediated myocardial injury. Am J Physiol Heart Circ Physiol 2005; 288: H2955-H2964.
[33] Su Y, Welch MJ and Shoghi KI. The application of maximum likelihood factor analysis (MLFA) with uniqueness constraints on dynamic cardiac microPET data. Phys Med Biol 2007; 52: 2313.
[34] Herrero P, Kim J, Sharp TL, Engelbach JA, Lewis JS, Gropler RJ and Welch MJ. Assessment of myocardial blood flow using ^{15}O-water and 1-^{11}C-acetate in rats with small-animal PET. J Nucl Med 2006; 47: 477-485.
[35] Faust A, Wagner S, Law MP, Hermann S, Schnockel U, Keul P, Schober O, Schafers M, Levkau B and Kopka K. The nonpeptidyl caspase binding radioligand (*S*)-1-(4-(2-[^{18}F] Fluoroethoxy)-benzyl)-5-[1-(2-methoxymethyl-pyrrolidinyl)sulfonyl]isatin ([^{18}F]CbR) as potential positron emission tomography-compatible apoptosis imaging agent. Q J Nucl Med Mol Imaging 2007; 51: 67-73.
[36] Ambrosio G, Weisman H, Mannisi J and Becker L. Progressive impairment of regional myocardial perfusion after initial restoration of post-ischemic blood flow. Circulation 1989; 80: 1846-1861.

Supplementary methods

Cell culture

HeLa cells were purchased from the Washington University Tissue Culture Support Center and cultured in Eagle's minimum essential medium (MEM) containing 10% heat-inactivated fetal bovine serum (FBS), 2 mM L-glutamine, 1 × non-essential amino acids (NEAA), and 1 × penicillin/streptomycin solution. HeLa cells were maintained in a 5% CO_2/95% humidified air atmosphere at 37°C.

In vitro caspase inhibition studies with ICMT-18

Enzyme inhibition assays were performed as previously reported (1). Briefly, recombinant human caspases (3, 6, and 8) and their peptide-specific substrates (Ac-DEVD-AMC, Ac-VEID-AMC, and Ac-IETD-AMC, respectively) were purchased from Sigma-Aldrich (St. Louis, MO) with the exception of caspase-1 and caspase-7 which were obtained from BIOMOL Research Laboratories (Plymouth Meeting, PA). Peptide specific substrates for caspase-1 and -7 (Ac-YVAD-AMC and Ac-DEVD-AMC) were also acquired from Sigma-Aldrich. The enzymatic activity of caspases was determined by measuring the accumulation of the fluorogenic product 7-amino-4-methylcoumarin (AMC). All assays were prepared in 96-well format at a volume of 210 µl per well and consisted of: 100 mM Na+ HEPES (pH 7.4), 10% sucrose, 100 mMNaCl, 0.1% CHAPS, 5 mM 2-mercaptoethanol, 2 mM EDTA, 10 µM Ac-YVAD-AMC (caspase-1); 20 mM Na+ HEPES (pH 7.4), 10% sucrose, 100 mMNaCl, 0.1% CHAPS, 2 mM EDTA, 10 µM Ac-DEVD-AMC (caspase-3); 20 mM Na+ HEPES (pH 7.4), 10% sucrose, 100 mM NaCl , 0.1% CHAPS, 2 mM EDTA, 10 µM Ac-VEID-AMC (caspase-6); 20 mM Na+ HEPES (pH 7.4), 100 mM NaCl, 10% sucrose, 0.1% CHAPS, 5 mM 2-mercaptoethanol, 2 mM EDTA, 10 µM Ac-DEVD-AMC (caspase-7); 20 mM Na+ HEPES (pH 7.4), 10% sucrose, 100 mM NaCl, 0.1% CHAPS, 2 mM EDTA, 10 µM Ac-IETD-AMC (caspase-8).

Recombinant caspases were first assayed to determine the optimal concentration for each experiment. Optimal concentrations were based in the linear range of the enzyme activation curves. Peptide inhibitors with known IC_{50} values were tested together with the compounds as a control for each caspase assay.Peptide inhibitors, Ac-DEVD-CHO (caspase-3 and -7), Ac-VEID-CHO (caspase-6), and Ac-IETD-CHO (caspase-8) were purchased from Sigma-Aldrich (St. Louis, MO) with exception of caspase-1 specific inhibitor (Ac-YVAD-CHO) which was acquired from BIOMOL Research Laboratories (Plymouth Meeting, PA). Peptide inhibitors and ICMT-18 were dissolved in DMSO and a serial dilution was performed prior to screening in order to obtain desired concentrations. 10 µl was added to each well containing 100 µl caspase solution and allowed to incubate on ice for 30 minutes. 100 µl substrate solution was added to each well and plates were incubated for 1-2 hours at 37°C. The final concentration of DMSO in all wells was 5% of the total volume.

The amount of AMC released was determined by using a Victor3 microplate fluorometer (Perkin Elmer Life Sciences, Boston, MA) at excitation and emission wavelengths 355 nm and 460 nm, respectively. Compounds were tested in duplicate and IC_{50} curves were calculated for all inhibitors assayed as previously described [1]. Final IC_{50}'s were the average of 3 independent experiments. The results are depicted in Supplemental Figure 3, Supplementary Materials.

In vitro cold competition cell uptake studies with [^{18}F]WC-4-116

HeLa cells were plated 2 × 10^5 cells per well in 12-well plates 24 hours prior to the cell uptake study, ensuring 70% confluency of the cells and complete adherence to the plate. Six hours before the initiation of the experiment, 2 µM of staurosporine was added to each well to induce apoptosis and caspase-3 activation. For cold competition studies, 5 µM unlabeled WC-4-116 was first added to selected wells prior to the administration of [^{18}F]WC-4-116. At time zero, 1 µCi [^{18}F]WC-4-116 (specific activity, 5480 mCi/µMol) was added to each well. After incubation of 5, 15, and 30 min the culture medium was removed and transferred into 2 ml microcentrifuge tubes for scintigraphic analysis. The cells were then washed once with 1 ml of cold phosphate buffered saline; the wash then collected for scintigraphy as well. The cells were lysed in the 12-well plates by treatment with 0.2% sodium dodecyl sulfate solution.

The cell lysates were harvested and the radioactivity content of the culture medium, wash, and cellular lysate were measured using a 1480 Wizard2 gamma counter (Perkin Elmer, Turku, Finland). The assay was performed in triplicate and results are reported as counts per min (CPM) of activity in the cell lysates for the samples with and without excess (unlabelled) WC-4-116 and depicted in Supplemental Figure 4, Supplementary Materials.

Quantitation of at-risk myocardial blood flow of IR and SS animals

See microPET imaging protocol section in Methods for details. Mean myocardial blood flow ± standard errorof the at-risk left ventricular region was assessed by adjunctive [^{15}O]H_2O microPET imaging for the IR and SS animals prior to the administration of either [^{18}F]WC-4-116 or [^{18}F]ICMT-18. All treatments are n = 4 except for the SS group imaged with [^{18}F]WC-4-116 (n = 3), with a *p*-value (ANOVA) = 0.29 for interaction between radiotracer and treatment type. The results are depicted in Supplemental Figure 6, Supplementary Materials.

Reference

[1] Chu W, Rothfuss J, Chu Y, Zhou D, Mach RH. Synthesis and in vitro evaluation of sulfonamide isatin Michael acceptors as small molecule inhibitors of caspase-6. J Med Chem. Apr 23 2009; 52: 2188-2191.

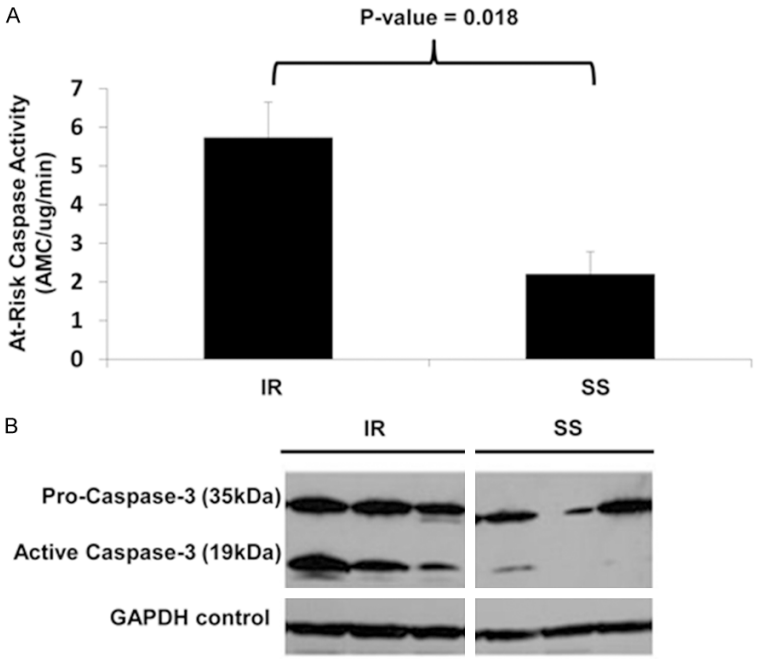

Supplement Figure 1. The *in vivo* LAD ligation model produces increased caspase-3 activity and expression. Panel A. Mean caspase-3/7 activity (± standard error) is elevated in the at-risk myocardium of the IR animals (n = 5) compared with the SS animals (n = 3). B. Western immunoblotting demonstrates enhanced expression of the active caspase-3 19 kDa fragment in the at-risk myocardial tissue samples for the IR but not the SS animals. Expression of the 35 kDA pro-caspase fragment and GADPH loading control are similar between treatments. AMC and GADPH denote amido-4-methylcoumarin and glyceraldehyde 3-phosphate dehydrogenase respectively.

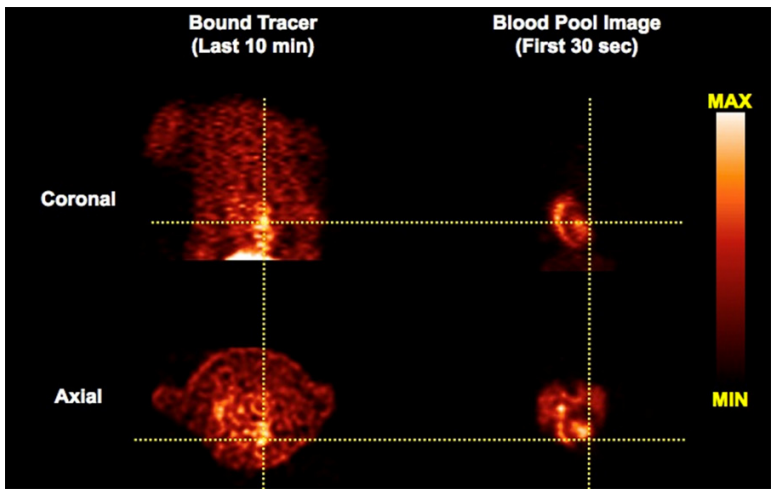

Supplemental Figure 2. Summed images late (left) and early (right) to differentiate tracer uptake in the myocardium and in the blood pool.

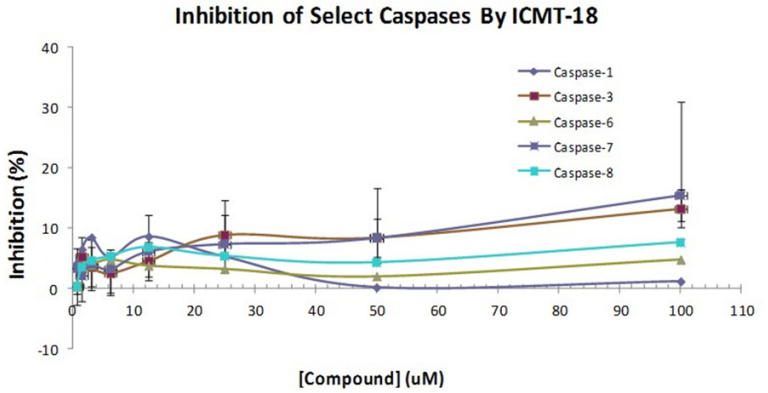

Inhibition of select caspases by ICMT-18

Caspase	Inhibition @ 100μM (%)
Caspase-1	2.3 ± 0.9
Caspase-3	15.3 ± 2.7
Caspase-6	5.8 ± 2.1
Caspase-7	18.4 ± 4.4
Caspase-8	7.8 ± 1.5

Supplemental Figure 3. Inhibition studies of caspases 1, 3, 6, 7, and 8 with ICMT-18. As expected, ICMT displayed no inhibition of caspase activity at a concentration up to 100 mM.

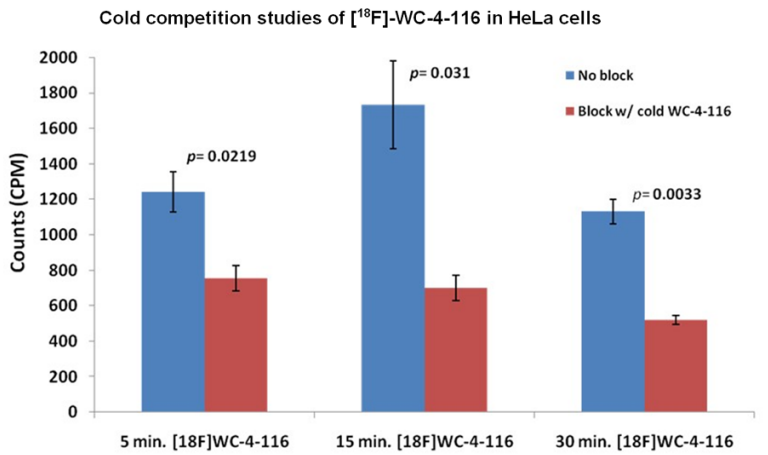

Uptake of compound measured in counts (CPM)		
Incubation Time	No Block	Block w/WC-4-116
5 min. [^{18}F]WC-4-116	1242 ± 112	758 ± 72
15 min. [^{18}F]WC-4-116	1734 ± 246	702 ± 74
30 min. [^{18}F]WC-4-116	1132 ± 70	521 ± 26

Supplemental Figure 4. Blocking studies in staurosporine-treated HeLa cells. Addition of unlabeled WC-4-116 is consistent with carrier-added blocking of caspase-3.

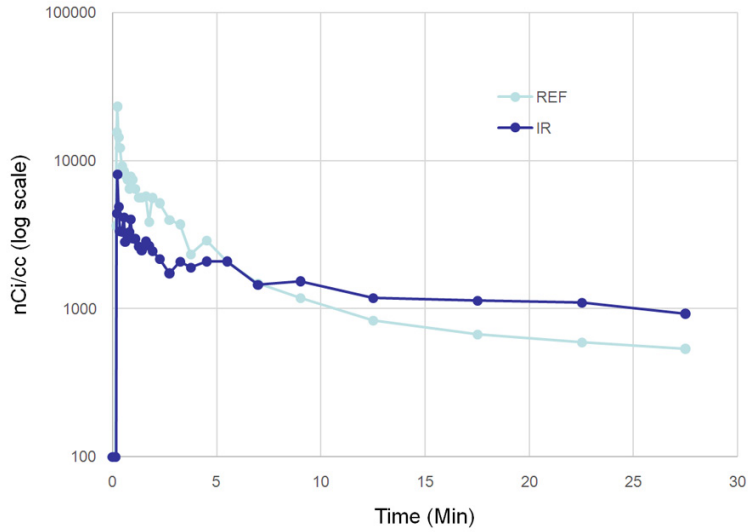

Supplemental Figure 5. Log-scale of TAC to highlight 2-fold ratio between IR and reference region at late time points.

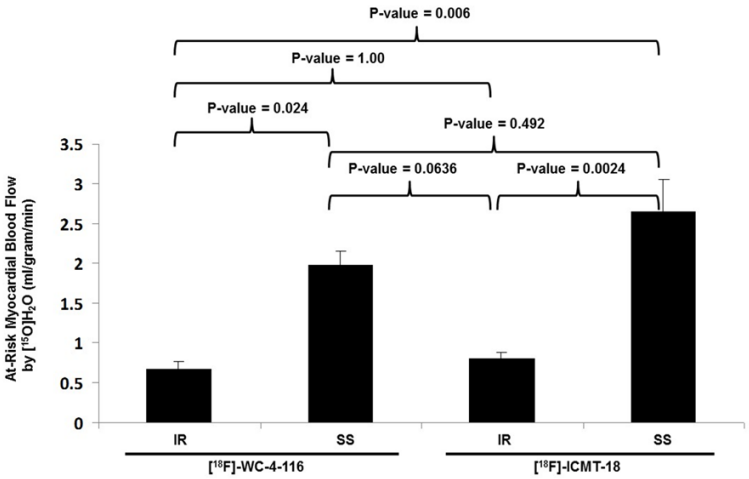

Supplemental Figure 6. [^{15}O]H_2O blood flow studies in IR and sham surgery controls. Although the IR animals had lower blood flow in the region at risk relative to the sham surgery controls, there was no difference in blood flow between the animals receiving [^{18}F]WC-4-116 versus [^{18}F]ICMT-18 (*P* value = 1.00). These data confirm that the increase uptake of [^{18}F]WC-4-116 versus [^{18}F]ICMT in the region at risk in the IR animals is due to binding to activated caspase-3 and not due to differences in myocardial blood flow.